

RESEARCH ARTICLE

Flexibility Analysis and Experimental Design of Dual-Chamber Bellows Isolator for Low-Frequency Damping Performance

MIAOLONG CAO^{1,2}, YUZHOU SUN², QINGYU DU³, AND ZIJIAN YING⁴¹Faculty of Mechanical Engineering and Automation, Zhejiang University of Science and Technology, Hangzhou 310018, China²School of Mechanical and Energy Engineering, Zhejiang University of Science and Technology, Hangzhou 310023, China³Han Meilin Art Museum, Hangzhou 310013, China⁴Faculty for Informatics, Ostfalia University of Applied Sciences, 38302 Wolfenbüttel, Germany

Corresponding author: Miaolong Cao (cml_q@163.com)

This work was supported in part by the Natural Science Foundation of Zhejiang Province under Grant LQY19E050001.

ABSTRACT To achieve an effective and versatile solution for reducing vibrations and reducing maintenance costs, the dual-chamber flexible bellows isolator (D-CFBI) of rubber material is designed. The outer chamber of D-CFBI is used as an actuator to change its own variable stiffness and control the feedback force by filling negative pressure gas. The inner chamber is used as a rubber air spring to work as the main vibration isolation element. Under different loads and sinusoidal excitation forces, the damping characteristics and damping effects of the D-CFBI with different stiffness are investigated. By exciting the isolator, the frequency sweep experiment is carried out, the dynamic flexibility in the initial state is studied, and a preload of the D-CFBI is given to change the stiffness of the D-CFBI, and the changing trend between restoring force and amplitude and frequency is found out. Conclusions can be summarized that increasing the preload of the D-CFBI leads to increased stiffness and better damping effect. For compression amounts of 20% and frequencies higher than 7Hz or amplitudes lower than 2mm, the damping effect is also better. Consequently, this D-CFBI offers satisfactory damping and increased safety at low amplitudes and frequencies. To achieve optimal damping, it is recommended to adjust the stiffness of the driver.


INDEX TERMS Flexible isolator, bellows, vibration damping performance, energy consumption.

I. INTRODUCTION

Vibration isolation is a method to reduce the impact of harmful vibration of the vibration source on the load equipment. The vibration isolation device is placed between the vibration source and the load equipment, and the elastic deformation of the vibration isolation device is used to consume the energy of vibration. The vibration isolation device is called the vibration isolator [1]. Vibration isolator is mainly composed of air spring structure, pendulum structure and active control system. Air spring is a rubber device that uses the viscoelasticity of rubber and the compressibility of gas volume to realize the spring effect. It has many superior physical characteristics, such as almost constant natural frequency and

low stiffness of spring under large load [2]. In recent years, for the lightweight, high-speed and comfortable requirements of the vehicle increase, air spring is often used as an elastic component in the suspension system of the vehicle [3]. The design of air springs may vary according to the application, and the design differences will affect the performance of air springs, which can be divided into two main types: rolling vane type and bellows type [4].

Bellows type air spring has various characteristics such as pressure resistance and impact resistance, and its multiple transverse lines have good vibration reduction effect [5]. According to different materials, common bellows can be divided into metal bellows and rubber bellows [6]. Metal bellows have good anisotropy and noise reduction performance, and can expand irregularly and absorb energy [7]. Compared with traditional vibration damping devices, metal bellows are

The associate editor coordinating the review of this manuscript and approving it for publication was Yingxiang Liu .

also light in weight, so they can be widely used in aerospace, pipeline system, agriculture and other fields [8], [9]. Due to its low manufacturing cost, good elastic performance and vibration reduction characteristics, rubber bellows are often used as elastic sensitive components, mechanical seal components, dielectric vibration isolation components, etc. [10], and can be used in instrument control, mechanical arm end and other positions, such as connecting pipes, gas fingers, etc. [11], [12]. Jiao et al. [13] established a simulation pipeline system. When the internal viscosity of the silicone oil is low, the bellows model has stable hydraulic stiffness in the middle and high frequency domain. Gao and Teng [14] et al. designed a new type of oil-gas isolator to solve the problem of low-frequency interference. At the same time, the variation trend of nonlinear stiffness is studied by the volume proportion of different media in the bellows. Due to the elasticity of its material, the bellows of rubber material have better variable stiffness capability, provide excellent flexibility and vibration damping, and are more suitable for application as air springs in vibration isolation scenarios.

To better verify the dynamic experimental results, Chen et al. [15] proposed a nonlinear hysteresis model for rubber bellows and established a rolling lobe air spring (RLAS) stiffness model. Shen et al. [16] developed a nonlinear model for metal rubber bellows and verified it through dynamic experiments. Hua et al. [17] studied the stiffness characteristics of bellows-type hoses and explored their mechanical model when reaching balance under internal pressure. Huo et al. [18] researched the displacement compensation ability of reinforced S-shaped bellows under different stiffness and analyzed its vibration reduction effect. Gawande and Pagar [19] found that reducing the axial natural frequency of U-shaped bellows can avoid resonance through analyzing their dynamic characteristics. Shi et al. [20] explored the dynamic changes of multiple bellows and their influencing factors on vibration reduction. These studies provide useful information for bellows' dynamic and stiffness characteristics, hysteresis, and vibration reduction effect, emphasizing the importance of an accurate nonlinear model for verifying test results of rubber bellows.

Similarly, when controlling devices such as manipulators, flexible bellows are used to better solve the problem of excessive displacement in order to better reduce the impact of oscillation on working accuracy [21], [22], [23]. Yang et al. [7] compared double-layer metal, rubber, and coated rubber bellows' vibration control in seawater. Flexible bellows isolators can link the mechanical arm and claw to control movement and reduce robot end vibration. Yu et al. [24] proposed solid-liquid bellows to isolate low-frequency vibration. These studies show that bellows shaped air springs have good performance as vibration isolation devices and have been widely used.

A previous study identified factors affecting bellows displacement and contraction through simulations [25]. This paper design a dual-chamber flexible bellows

isolator (D-CFBI) with Thermoplastic Elastomer (TPE) material to achieve cost-effectiveness, reliability, and environmental adaptability. Experiments and simulations investigate the D-CFBI's vibration dampness and excitation frequency relationship, finding its damping range varies with excitation frequency and amplitude. The experiment tests the D-CFBI's dynamic flexibility in the initial state and with different preloads to obtain varied damping effects. The relationship between pre pressure and vibration reduction effect is compared to find the best effect under different pre pressure.

II. DESIGN AND MATHEMATICAL MODEL OF D-CFBI

A. STRUCTURAL PARAMETERS OF DUAL-CHAMBER BELLOWS

A two-cavity flexible bellows isolator is proposed in order to improve the damping degree and stability of the system and achieve the function of active vibration isolation. Both inner and outer cavities are closed cavities made of TPE material. The structure of the isolator is shown in Figure 1(a). The outer cavity is connected with the left and right holes for ventilation. The vibration state of the system can be measured by the sensor to control the contraction or expansion of the outer cavity, and then change the stiffness and damping of the rubber bellows. In this way, the feedback control force is applied to the system to achieve active vibration isolation. The aeration of the inner cavity makes it play a vibration isolation effect mainly as a rubber air spring. The inner cavity also limits the overall radial deformation of D-CFBA and prevents the non-axial displacement of D-CFBA during operation, thus affecting the damping effect.

D-CFBI is mainly assembled by a dual-chamber bellows body and a bellows end cover. They are integrally formed by 3D printing technology, and the connection between the end cover and the bellows is an interference fit. The outer hole size of the end cover is slightly larger than the inner circumference of the double cavity bellows connection, because this structure can be used in the double cavity bellows after the same period. The generated internal pressure presses the bellows against the end cover, thereby increasing the friction between the end cover and the bellows, improving the pressure bearing capacity of the isolator, and ensuring its sealing. The D-CFBI is made of TPE material that is a kind of rubber-like material with good geometric nonlinear characteristics. Compared with traditional rubber materials, TPE has good tensile strength and elongation at break, which makes it better absorb the energy transferred in the vibration to achieve better vibration damping effects. Most importantly, and due to its low price and thermoplastic, TPE material can be reused, which meets the requirements of the D-CFBI.

B. MATHEMATICAL MODEL OF THE DUAL-CHAMBER FLEXIBLE BELLOWS ISOLATOR

To study the effect of excitation magnitude on stiffness and damping, a mechanical model is established and the stiffness softening and damping strengthening effects are

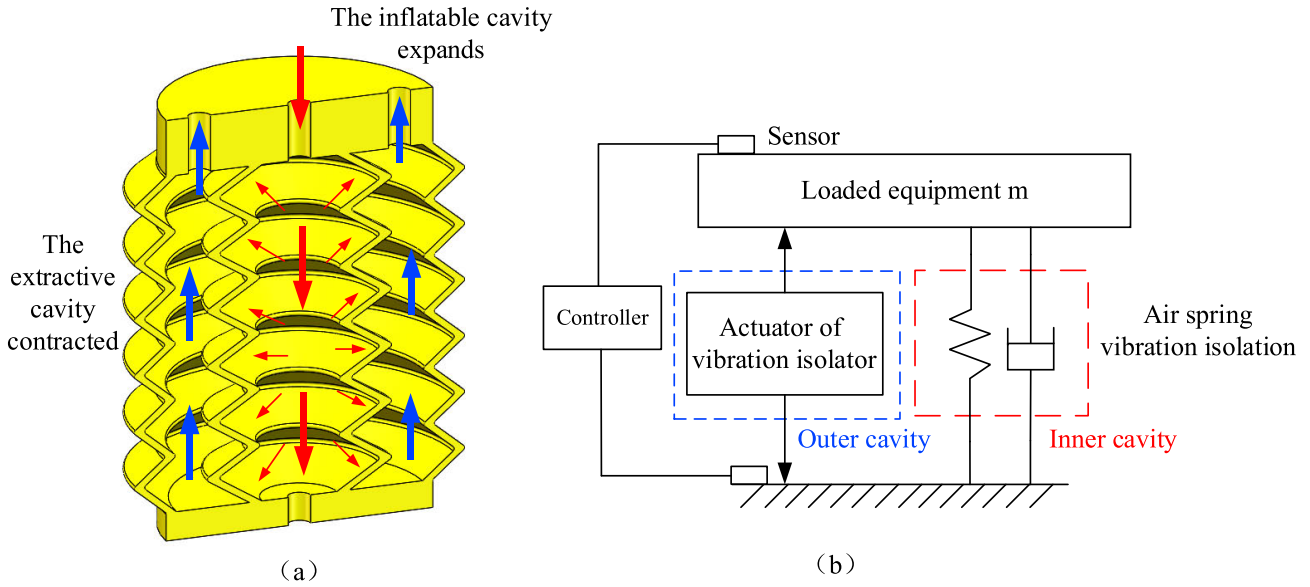


FIGURE 1. Modeling diagram of the dual-chamber flexible bellows isolator: (a) Section diagram of D-CFBI; (b) Diagram of the vibration isolator.

explained theoretically. The bellows rubber damping structure system exhibits nonlinear hysteresis characteristics of variable damping and variable stiffness, and its elastic restoring force contains various components. When the bellows system is sinusoidally excited by $F = F_0 \sin \omega t$, the hysteresis vibrator model can be used to describe the nonlinear elastic restoring force system. The elastic resilience includes non-memory links and memory links, as shown in Figure 1(b). To better establish a restoring force model and explain the stiffness softening and damping strengthening effects, the high-order nonlinear elastic restoring force with more than three memory-free links is ignored, and the elastic restoring force model can be described by Equation (1):

$$m\ddot{x} + c\dot{x} + kx + z(t) = F_0 \sin \omega t \quad (1)$$

Introducing variable:

$$2\xi = \frac{c}{m}, \omega_0^2 = \frac{k}{m}, \tilde{F} = \frac{F_0}{m} \quad (2)$$

From Equations (1) and (2):

$$\ddot{x} + 2\xi\dot{x} + \omega_0^2 x + \frac{1}{m}z(t) = \tilde{F} \sin \omega t \quad (3)$$

Although the hysteresis oscillator response contains higher harmonics, a large number of experiments prove that the fundamental wave component plays a dominant role. The higher harmonics are ignored, and the solution is set as:

$$x = x_m \sin(\omega t + \varphi_x) \quad (4)$$

where: x_m is displacement amplitude; ω is the excitation frequency; φ_x is the initial phase angle.

The memory link model considered to be equivalent to the parallel structure of linear viscous damping and spring:

$$z(x, \dot{x}) = c_{eq}\dot{x} + k_{eq}x \quad (5)$$

According to Equation (4):

$$\dot{x} = x_m \omega \cos(\omega t + \varphi_x) \quad (6)$$

Substitute x, \dot{x} concrete expression into Equation (5) to obtain:

$$z(x, \dot{x}) = c_{eq}x_m \omega \cos(\omega t + \varphi_x) + k_{eq}x_m \sin(\omega t + \varphi_x) \quad (7)$$

Trig transformation is carried out on both sides of Equation (7), the orthogonal property of trigonometric function is considered, and the average operation can be obtained:

$$\begin{aligned} & \frac{1}{2\pi} \int_{\varphi_x}^{\varphi_x+2\pi} c_{eq}x_m \omega \cos^2(\omega t + \varphi_x) d(\omega t) \\ &= \frac{1}{2\pi} \int_{\varphi_x}^{\varphi_x+2\pi} z(x, \dot{x}) \cos(\omega t + \varphi_x) d(\omega t) \end{aligned} \quad (8)$$

Lead-in coordinate transformation:

$$\begin{aligned} & \frac{1}{2\pi} \int_{\varphi_x}^{\varphi_x+2\pi} c_{eq}x_m \omega \sin^2(\omega t + \varphi_x) d(\omega t) \\ &= \frac{1}{2\pi} \int_{\varphi_x}^{\varphi_x+2\pi} z(x, \dot{x}) \sin(\omega t + \varphi_x) d(\omega t) \end{aligned} \quad (9)$$

Then Equation (4) becomes:

$$\tau = t - t_s, t_s = \left(\frac{\pi}{2} - \varphi_x\right) \frac{1}{\omega} \quad (10)$$

Under sinusoidal displacement loading, memory restoring force $z(t)$ and relative displacement $x(t)$ form a double-broken

functional constitutive relationship:

$$x = x_m \sin(\omega t + \varphi_x) = x_m \cos \omega \tau = x_m \cos \tilde{\theta} \quad (11)$$

From Equation (12):

$$x_m - 2x_s = x_m \cos \theta \quad (12)$$

And the expression of $z(\tau)$ in the above intervals can be obtained by derivation. The double-broken hysteretic restoring force $z(\tau)$ is a function of period 2π .

$$\theta = \arccos\left(1 - \frac{2x_s}{x_m}\right) \quad (13)$$

According to Equations (10), (11), (13):

$$\begin{aligned} & \frac{1}{2\pi} \int_{\varphi_x}^{\varphi_x+2\pi} z(x, \dot{x}) \cos(\omega t + \varphi_x) d(\omega t) \\ &= \frac{1}{2\pi} \int_{\varphi_x}^{\varphi_x+2\pi} z(x, \dot{x}) \sin \tilde{\theta} d\tilde{\theta} = \frac{4z_s}{2\pi} \left(1 - \frac{x_s}{x_m}\right) \end{aligned} \quad (14)$$

$$\begin{aligned} & \frac{1}{2\pi} \int_{\varphi_x}^{\varphi_x+2\pi} z(x, \dot{x}) \sin(\omega t + \varphi_x) d(\omega t) \\ &= \frac{1}{2\pi} \int_{\varphi_x}^{\varphi_x+2\pi} z(x, \dot{x}) \cos \tilde{\theta} d\tilde{\theta} = \frac{k_s x_m}{2\pi} \left(1 - \frac{x_s}{x_m}\right) \end{aligned} \quad (15)$$

Equation (14) is substituted into Equation (8), and the left side of Equation (8) is simply integrated to sort out:

$$c_{eq} = \frac{4z_s}{\pi \omega x_m} \left(1 - \frac{x_s}{x_m}\right) \quad (16)$$

Similarly, Equation (15) is substituted into Equation (9), and simple integral operation is performed on the left side of Equation (9):

$$k_{eq} = \frac{k_s}{\pi} (\theta - \sin \theta \cos \theta) \quad (17)$$

When $x_m/x_s \rightarrow \infty$, $n_c = (\pi \omega x_m / 4z_s) c_{eq} \rightarrow 1$, $n_k = (\pi/k_s) k_{eq} \rightarrow 0$, that is, equivalent viscous damping coefficient $c_{eq} \rightarrow 4z_s / \pi \omega x_m$, equivalent stiffness $k_{eq} \rightarrow 0$. Therefore, it can be inferred theoretically that the stiffness of bellows rubber structure decreases with the increase of excitation amplitude, while the damping increases, which is consistent with the experimental results, and can reasonably explain the stiffness softening and damping strengthening effects of bellows metal rubber cladding damping structure.

In addition, the proposed vibration isolator consists of a spring system with damping and an actuator, which can also be seen as a rubber spring with damping. The mathematical models of them are similar. Inner cavity can be viewed as an air spring, when the air spring with vertical load change and cause a balloon height change (air spring is compressed or stretched), the volume and pressure inside the balloon also produces change, gas state equation is as follows:

$$(p + p_a) V^n = (p_0 + p_a) V_0^n \quad (18)$$

where, p_a is the atmospheric pressure, p_0 and V_0 are the pressure and volume in the air spring of standard height, p and V are the pressure and volume in the air spring of any height, n is the variable index, whose value is related to the deformation speed of the air spring will. The spring force of the air spring is:

$$F = \left[\left(\frac{V_0}{V} \right)^n (p_0 + p_a) - p_a \right] A_e \quad (19)$$

Air spring volume V , the effective area of A_e are gasbag internal pressure p and the function of the air spring deformation x , $V = V(p, x)$ and $A_e = A_e(p, x)$, because of the influence of pressure on the volume and effective area is small, analysis does not consider.

By derivation of Equation (2) with travel x , stiffness characteristics of air spring are obtained:

$$\begin{aligned} K = \frac{dF}{dx} &= -n(p_0 + p_a) A_e \frac{V_0^n}{V^{n+1}} \\ &+ \left[\left(\frac{V_0}{V} \right)^n (p_0 + p_a) - p_a \right] \frac{dA_e}{dx} \end{aligned} \quad (20)$$

Material in the process of the micro vibration where $V_0/V = 1$ and use $A_e = -dV/dx$, (3) becomes:

$$K = n(p_0 + p_a) \frac{A_e^2}{V_0} + p_0 \frac{dA_e}{dx} \quad (21)$$

$K_1 = n(p_0 + p_a)(A_e^2/V_0)$ is related to loading (static or dynamic) and shape of the structure parameters (effective area and volume); $K_2 = p_0(dA_e/dx)$ is associated with the changing rule of the effective area.

According to equation (4), the vibration frequency of the air spring is:

$$f = \frac{1}{2\pi} \sqrt{\frac{K}{M}} = \frac{1}{2\pi} \sqrt{ng \left(1 + \frac{p_a}{p_0} \right) \frac{A_e}{V_0} + \frac{g}{V_0} + \frac{g}{A_e} \left(\frac{dA_e}{dx} \right)} \quad (22)$$

where, g is the acceleration of gravity; M is the air spring bearing mass.

III. MATHEMATICAL MODEL OF THE DUAL-CHAMBER FLEXIBLE BELLOWS ISOLATOR

A. EXPERIMENTAL PROCESS AND PRINCIPLE

According to the above theory, D-CFBI will produce stiffness softening and damping strengthening effects when the excitation magnitude increases to a certain extent. To study the influence of excitation magnitude on the stiffness and damping of D-CFBI damped structure, and obtain the amplitude-frequency characteristic curve of D-CFBI damped structure, it is necessary to apply external sinusoidal excitation to D-CFBI, and collect the excitation force signal and the vibration amplitude displacement signal of the bellows metal-rubber clad damped structure. This study mainly aimed to obtain the resonant frequency of the D-CFBI through forward and reverse frequency sweeps. To obtain the damping structure spectral characteristic curve of the D-CFBI, it is

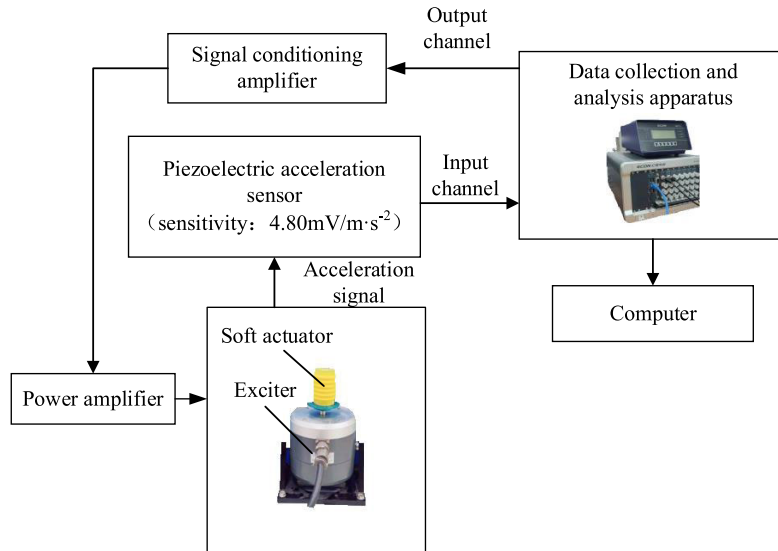


FIGURE 2. Schematic diagram of the frequency sweep experiment of the dual-chamber.



FIGURE 3. The dynamic experimental device of the dual-chamber flexible bellows isolator.

necessary to compare the isolator in different states. The external sinusoidal excitation is applied, and the displacement signal of the vibration amplitude of the D-CFBI is collected. By sweeping the D-CFBI, its resonance frequency is found, and by replacing the sensor, the physical characteristics such as hysteresis loop can be further measured. The loss factor and other parameters are calculated under different conditions to compare the quality of the damping performance. The dynamic experimental system of the D-CFBI is dominantly composed of a data acquisition and analyzer (ECON-MI-8008, 47-63Hz), a power amplifier (ECON-MI-2004, DC 12-28V), a vibration exciter (E-JZK-10), a dual-chamber bellows, and a PC terminal. The experimental principle is displayed in Figure 2. A sine frequency sweep signal is generated through a data acquisition and analyzer; the signal stability is adjusted through a signal conditioning amplifier; the signal is amplified by the signal amplifier; the amplified signal is transmitted to the vibration exciter to make

a D-CFBI receive the stable sinusoidal dynamic excitation that is provided by the vibration exciter; and, finally, the signal is transmitted to the data acquisition and analyzer and viewed by the PC. The dynamic experimental device of the dual-chamber flexible bellows isolator is shown in Figure 3. The data acquisition system obtains the resonant frequency of the D-CFBI by analyzing the collected system input and output signals. Meanwhile, in the actual work process, the load or amplitude is further changed, and the force signal and displacement signal of the D-CFBI are collected.

B. ANALYSIS ON EXPERIMENTAL RESULTS

The evaluation of the dynamic characteristics of the D-CFBI examines its ability to resist vibration. Therefore, the dynamic flexibility formula is introduced:

$$R = \frac{L}{F} \tag{23}$$

where is dynamic flexibility, as the value of dynamic flexibility is smaller, the ability to resist vibration is better. The relative displacement between the end of the driver spindle and the exciter caused by the exciting force is expressed by L and F is the magnitude of exciting force. When the exciting force is constant, if the value of L is smaller, the value of R is smaller, indicating that the better the dynamic performance of the driver.

A dynamic sine frequency sweep experiment is performed on the axial direction of the D-CFBI. The excitation force is kept unchanged, with the sweep from low frequency to high frequency (5~500 Hz), and the amplitude-frequency change image in the process of frequency sweep is derived; with the sweep being reversed from high frequency to low frequency (500~5 Hz); the amplitude frequency is recorded when reversing sweep.

When the given excitation force is 2N, the sweep frequency experiment results of the D-CFBI are exhibited in Figure 4. Among them, the black curve represents the relationship between dynamic compliance and frequency when sweeping forward, and the red curve refers to the relationship between dynamic compliance and frequency when sweeping backward. Dynamic flexibility is used as a measure of the isolator's stiffness in this study because it provides a more comprehensive understanding of the isolator's behavior than just looking at displacement transmissibility alone. Dynamic flexibility takes into account both the stiffness and the damping of the isolator, which are both important factors in determining its overall vibration isolation performance.

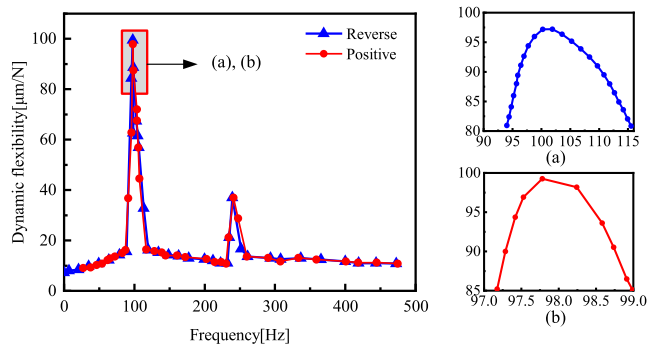


FIGURE 4. Sweep frequency curve of the dual-chamber flexible bellows isolator at 2N.

According to Figure 4, its resonant frequency is around 98Hz. When the frequency is swept forward, the peak value is at 98.968Hz, and the dynamic flexibility is $97.345\mu\text{m}/\text{N}$ at this time. And when sweeping the frequency in the reverse direction, the peak value is obtained at 97.7995Hz, and the dynamic flexibility is $99.467\mu\text{m}/\text{N}$ at this time. This conclusion shows that under normal pressure, the D-CFBI can effectively avoid the resonance phenomenon in the low frequency range. The conclusion also shows that the resonant frequency of forward sweep is slightly larger than that of reverse sweep, but the dynamic flexibility is relatively smaller. This is due

to the phenomenon of bending and jumping in the frequency response curve.

In the frequency sweep process, if the given excitation force increases, the excitation force increases to 5N and 7N, respectively. The comparison chart of the frequency sweep is demonstrated in Figure 5.

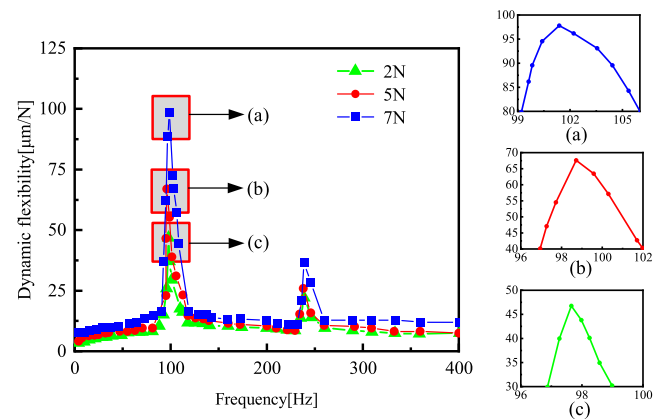


FIGURE 5. Sweep frequency curves of the dual-chamber flexible bellows isolator under different excitation forces.

As displayed in Figure 5, when the excitation force changes, the resonance peak of the sweep frequency curve with a larger exciting force is higher than that with a smaller exciting force, and the resonance frequency is also larger. When the excitation force is 2N, 5N and 7N respectively, the resonance frequencies at the peak are 97.968Hz, 97.618Hz and 97.493Hz respectively, and the dynamic flexibility is $98.345\mu\text{m}/\text{N}$, $67.164\mu\text{m}/\text{N}$ and $46.95\mu\text{m}/\text{N}$ respectively. Therefore, it can be explained that the D-CFBI has softened rigidity and increased damping.

IV. ANALYSIS OF DAMPING ENERGY DISSIPATION CHARACTERISTICS

Based on the tooling experiment test, if the experiment provides a constant frequency sinusoidal excitation to the D-CFBI and measures the hysteresis loop formed by the hysteresis to restore force and displacement, through the damping energy consumption ΔW and equivalent stiffness K_{eq} , the structural loss factor η and other concepts are quantitatively analyzed to further describe the damping effects and vibration reduction effects of the D-CFBI. When a constant frequency is provided, the dynamic stiffness can reflect the ratio of the amplitude of the response displacement to the amplitude of the load. If the structure loss factor is larger, it indicates that the material has better vibration damping effects, and the amount of energy dissipation is mainly expressed by the damping energy consumption ΔW that is represented by the area of the hysteresis loop. When the area of the hysteresis loop increases, it suggests that the internal friction value generated by the material increases and the damping effects are better.

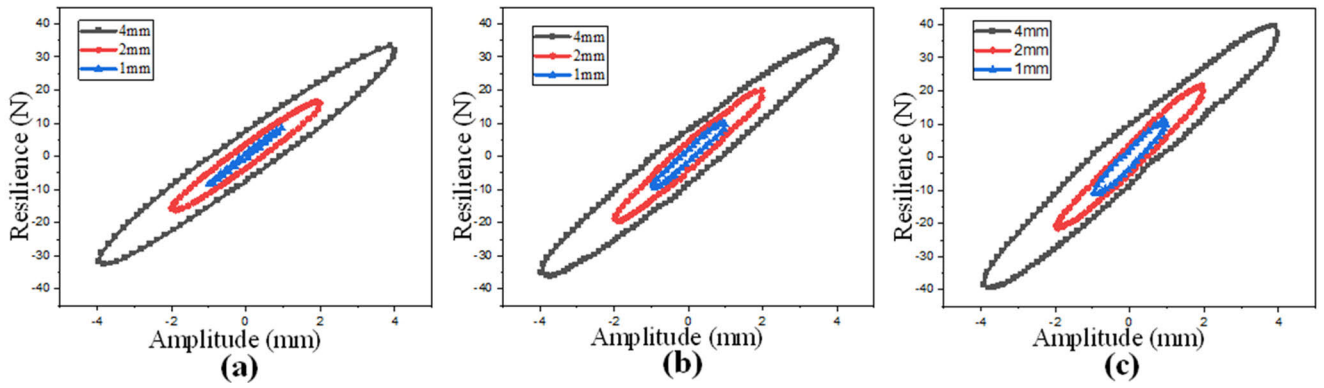


FIGURE 6. 7Hz magnetic hysteresis loop under different pre-pressure and different amplitude: (a) is under the initial shape, (b) is under the 10% compression, and (c) under the 20% compression.

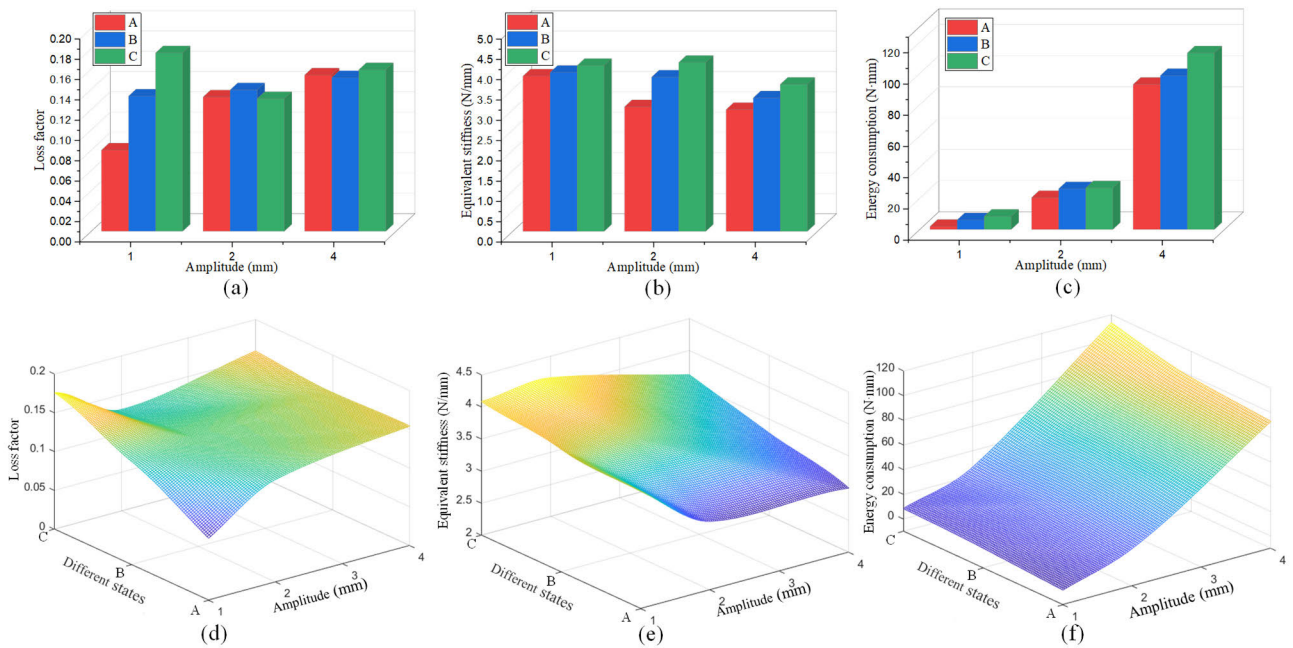


FIGURE 7. Comparison of digital models under different pre-pressures and amplitudes at 7Hz. (a) is under the initial shape, (b) is under the 10% compression and (c) is under the 20% compression.

A. DYNAMIC STIFFNESS EXPERIMENT AND COMPARISON

The dynamic characteristics of the D-CFBI is experimentally explored. In view of the excellent variable stiffness characteristics of TPE material, during the experiment, when a certain preload is applied to change the compression deformation of flexible double cavity bellows to 10% and 20%, the dynamic characteristic experiments under different stiffness are carried out respectively. Considering that the D-CFBI often works at low frequencies, it is based on 1mm, 2mm and 4mm, respectively, to better express the vibration damping situation. The hysteresis loops at different frequencies of 3Hz, 5Hz, 7Hz and 9Hz are compared. At the same time, the line graphs of loss factor, equivalent stiffness and energy consumption and their respective three-dimensional graphs are drawn, respectively.

When the frequency is 7Hz, the amplitude of the excitation is 1mm, 2mm and 4mm, respectively, and the hysteresis loop diagram can be obtained from the load and displacement data that are collected by the sensor, as shown in Figure 6:

On the basis of Figure 6, when the D-CBFA is under the initial shape, 10% compression and 20% compression, and when the excitation frequency is kept constant and the maximum amplitude of the vibration increases, the area of the hysteresis loop also increases: The energy consumption performance of the D-CFBI gradually increases.

For the typical hysteresis loop in Figure 6, the loss factor is calculated as:

$$\eta = \frac{\Delta W}{2\pi W} \tag{24}$$

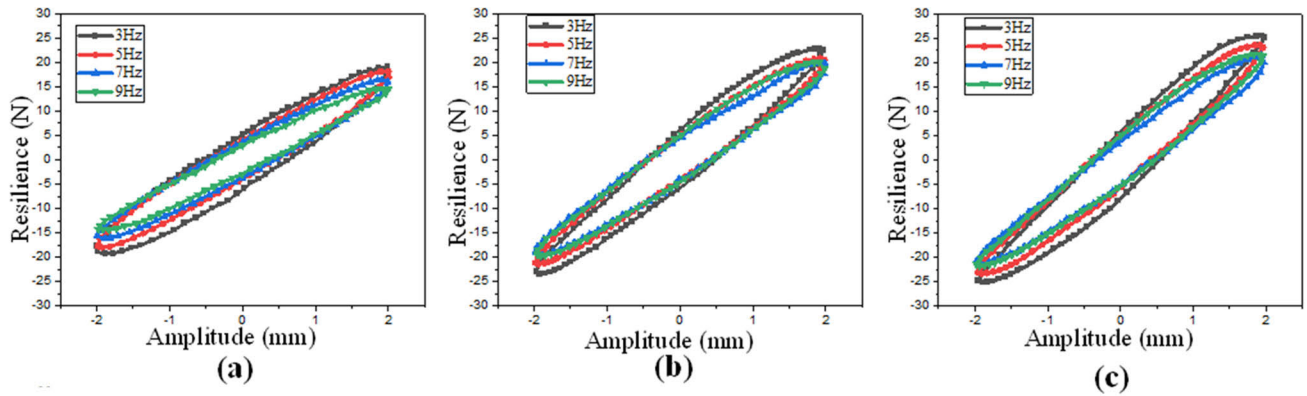


FIGURE 8. 2mm magnetic hysteresis loop under different pre-pressure and different amplitude: (a) is under the initial shape, (b) is under the 10% compression, and (c) is under the 20% compression.

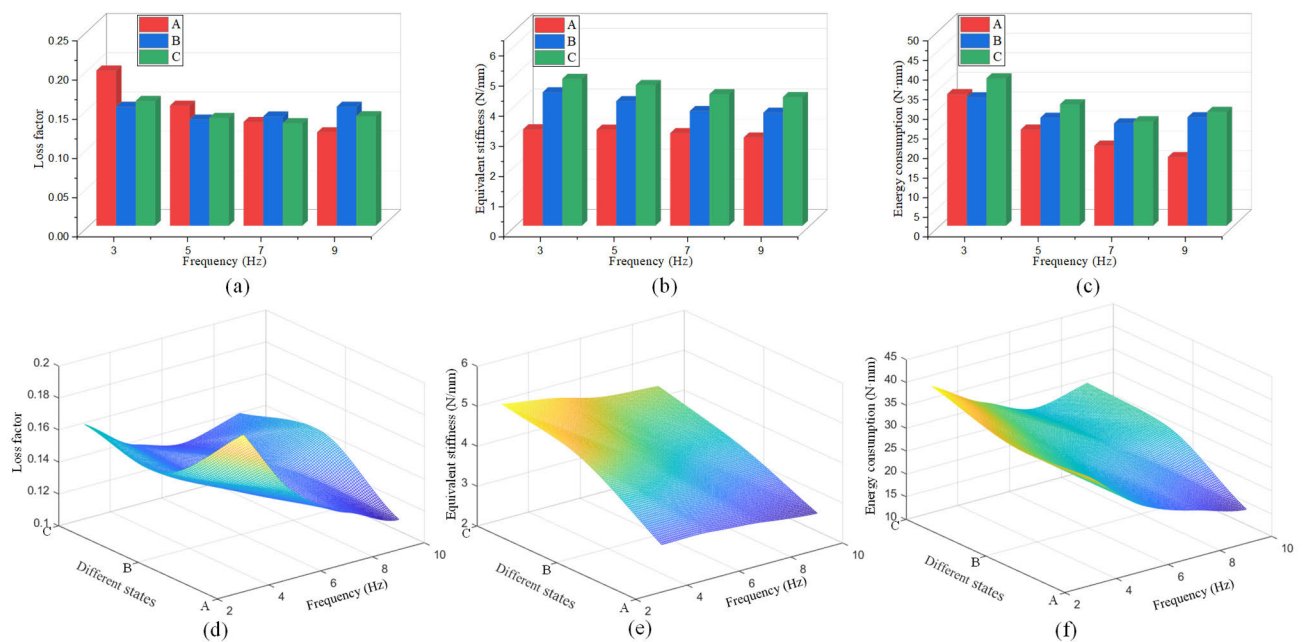


FIGURE 9. Comparison of digital models under different pre-pressures and amplitudes at 2mm. (a) is under the initial shape, (b) is under the 10% compression, and (c) is under the 20% compression.

The is the energy loss of the structure in one cycle, refers to the maximum strain energy stored in the structure.

The elastic potential energy is expressed as the equivalent dynamic stiffness:

$$W = \frac{(A_1 - A_2)^2}{2} K_{eq} \tag{25}$$

A_1 And A_2 are the maximum and the minimum amplitude during the experiment, respectively, so the dynamic stiffness can be expressed as:

$$K_{eq} = \frac{2W}{(A_1 - A_2)^2} \tag{26}$$

The hysteresis loops under different preloads in Figure 6 are calculated and solved respectively, the histogram graph

of average dynamic stiffness and loss factor can be obtained. In order to better see the changing trend, the author represents the loss factor, equivalent stiffness and energy consumption at different frequencies and amplitudes by three-dimensional graphs, and A, B, and C represent the amplitudes of the excitation amplitudes of 1mm, 2mm and 4mm respectively in Figure 7:

In the Figure 7, at low amplitude, the loss factor is greatly affected by the preload. When the compression is 20%, the loss factor is the largest, indicating that the vibration damping effect of the double cavity flexible bellows driver is the best. When the amplitude increases, there is little difference in the loss factors under several states. From the perspective of dynamic stiffness, the change trend of dynamic stiffness of the D-CFBI under different states is similar with the

increase of amplitude. On the whole, when the preload is the largest, the dynamic stiffness is the largest. In terms of energy consumption, with the increase of amplitude, the energy consumption is also increasing. When the preload is the largest, the energy consumption is the largest. Therefore, it can be explained that when the amplitude is 1 ~ 2mm, increase the preload to make the shape variable of the flexible double cavity bellows driver reach 20%. At this time, the vibration reduction effect is better than that of the case with small preload.

When maintaining the excitation amplitude at 2mm and changing the excitation frequency to 3Hz, 5Hz, 7Hz and 9Hz respectively, the hysteresis loop diagram in the Figure 8 below can be obtained:

According to Figure 8, as the excitation frequency increases, the slope of hysteresis loop decreases gradually. When the preload increases, the maximum restoring force required to reach the maximum amplitude increases. At this time, the slope of hysteresis loop increases gradually with the increase of preload. When substituting the measured values in the experiment into the digital model, the histogram of the average dynamic stiffness and loss factor can be obtained, and according to the numerical values at different frequencies, different three-dimensional diagrams are synthesized, as shown in Figure 9:

In Figure 9, as the excitation frequency increases, the loss factor in the initial state decreases gradually. When a certain preload is given, the loss factor decreases first and then increases. When the frequency is greater than 7Hz, the damping effect is better. The dynamic stiffness in different states shows a decreasing trend, but with the increase of preload, the dynamic stiffness also increases. Energy is lost more at low frequencies, which is because elastic materials absorb more energy at low frequencies, resulting in less energy being transmitted. In order to obtain the best damping effect under different excitation frequencies, it is necessary to consider the magnitude of pre-pressure.

V. CONCLUSION

In this present paper, the forward and reverse sweep frequency experiments are carried out for a new type of TPE material the D-CFBI. It is found that the D-CFBI has bending and jumping phenomenon, and the excitation magnitude of the sinusoidal excitation is changed, and the effects of stiffness softening and damping enhancement are observed as well. The phenomenon is explained by the hysteresis vibrator model, after which the relevant laws of excitation frequency and excitation magnitude on the vibration damping characteristics of the D-CFBI are investigated.

In the process of dynamic experiment, the dynamic softness of forward and reverse sweep frequencies is compared. It can be obviously proved that there is an obvious bending and jumping phenomenon in the D-CFBI. When reverse sweep frequency is conducted, the resonance frequency decreases, while the dynamic softness increases. By increasing the vibration magnitude, it can be observed

that the D-CFBI produces the effects of stiffness softening and damping enhancement. This is determined by the nature of the material itself.

Excitation experiments are performed on the axial direction of the D-CFBI. In the initial state, when the amplitude of the excitation is the same, as the excitation frequency increases, the energy consumption capacity and the loss factor reduce. When the frequency is kept constant and the vibration amplitude gradually increases within a certain range, its energy consumption capacity gradually increases, while the equivalent stiffness and the loss factor decrease. When the bellows works, the vibration amplitude is within 2-3mm and the vibration frequency is low frequency, the vibration reduction effect is the best.

During the dynamic experiment, properly increasing the pre-pressure can effectively improve the vibration reduction effect of the D-CFBI at low amplitude. Through digital theoretical calculation, it can be concluded that when the compaction deformation is 10%, the damping effect increases by 66.5% compared with the initial state, and when the compaction deformation is 20%, the damping effect increases by 31.98% compared with the compaction deformation of 10%.

At low frequency (3~5Hz), the loss factor in the initial state is better than that in the presence of pre-pressure, because the driver is made of TPE material, and the lagging vibration effect in the low frequency range is serious. At lower frequency (7~9Hz), the vibration reduction effect is better when the pre-pressure exists. Therefore, it can be shown that the pre-compaction driver has improved the vibration reduction effect.

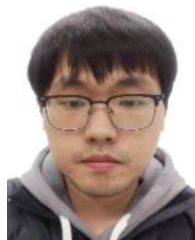
REFERENCES

- [1] I. Mendia-Garcia, N. Gil-Negrete Laborda, A. Pradera-Mallabiarrena, and M. Berg, "A survey on the modelling of air springs—Secondary suspension in railway vehicles," *Vehicle Syst. Dyn.*, vol. 60, no. 3, pp. 835–864, Mar. 2022.
- [2] Y. Zheng and W.-B. Shangguan, "A combined analytical model for orifice-type and pipe-type air springs with auxiliary chambers in dynamic characteristic prediction," *Mech. Syst. Signal Process.*, vol. 185, Feb. 2023, Art. no. 109830.
- [3] P. Pintado, C. Ramiro, A. L. Morales, A. J. Nieto, and J. M. Chicharro, "The dynamic behavior of pneumatic vibration isolators," *J. Vibrot. Control*, vol. 24, no. 19, pp. 4563–4574, Oct. 2018.
- [4] Z. Zhou, S. Chen, D. Xia, J. He, and P. Zhang, "The design of negative stiffness spring for precision vibration isolation using axially magnetized permanent magnet rings," *J. Vibrot. Control*, vol. 25, nos. 19–20, pp. 2667–2677, Oct. 2019.
- [5] G. P. Sreenivasan and M. M. Keppanan, "Analytical approach for the design of convoluted air suspension and experimental validation," *Acta Mechanica Sinica*, vol. 35, no. 5, pp. 1093–1103, Oct. 2019.
- [6] I. Dayyani, A. D. Shaw, E. I. S. Flores, and M. I. Friswell, "The mechanics of composite corrugated structures: A review with applications in morphing aircraft," *Compos. Struct.*, vol. 133, pp. 358–380, Dec. 2015.
- [7] Y. Yang, G. Pan, S. Yin, and Y. Yuan, "Experiment investigate on the effectiveness of flexible pipes to isolate sea-water pump generated vibration," *Coatings*, vol. 10, no. 1, p. 43, Jan. 2020.
- [8] F. S. Li, Q. Chen, and J. H. Zhou, "Dynamic properties of a novel vibration isolator with negative stiffness," *J. Vibrot. Eng. Technol.*, vol. 6, no. 3, pp. 239–247, Jun. 2018.
- [9] H.-M. Noh, "Improvement of transmission loss of bellows through thickness improvement and structural modification," *Adv. Mech. Eng.*, vol. 13, no. 9, Sep. 2021, Art. no. 168781402110496.

- [10] J. Liu, Y. Tong, Y. Liu, and Y. Liu, "Development of a novel end-effector for an on-orbit robotic refueling mission," *IEEE Access*, vol. 8, pp. 17762–17778, 2020.
- [11] R. MacCurdy, R. Katzschmann, Y. Kim, and D. Rus, "Printable hydraulics: A method for fabricating robots by 3D co-printing solids and liquids," in *Proc. IEEE Int. Conf. Robot. Autom. (ICRA)*, May 2016, pp. 3878–3885.
- [12] B. N. Peele, T. J. Wallin, H. Zhao, and R. F. Shepherd, "3D printing antagonistic systems of artificial muscle using projection stereolithography," *Bioinspiration Biomimetics*, vol. 10, no. 5, Sep. 2015, Art. no. 055003.
- [13] X. Jiao, J. Zhang, H. Zhao, and Y. Yan, "Research on dynamic stiffness of the damping element in bellows-type fluid viscous damper by a simplified model," *Eng. Comput.*, vol. 38, no. 1, pp. 413–441, Jan. 2021.
- [14] X. Gao and H. D. Teng, "Dynamics and isolation properties for a pneumatic near-zero frequency vibration isolator with nonlinear stiffness and damping," *Nonlinear Dyn.*, vol. 102, no. 4, pp. 2205–2227, Dec. 2020.
- [15] J.-J. Chen, Z.-H. Yin, X.-J. Yuan, G.-Q. Qiu, K.-H. Guo, and X.-L. Wang, "A refined stiffness model of rolling lobe air spring with structural parameters and the stiffness characteristics of rubber bellows," *Measurement*, vol. 169, Feb. 2021, Art. no. 108355.
- [16] G. Shen, M. Li, and X. Xue, "Damping energy dissipation and parameter identification of the bellows structure covered with elastic-porous metal rubber," *Shock Vibrat.*, vol. 2021, pp. 1–12, Feb. 2021.
- [17] G. Hua, S. Changgeng, and X. Guomin, "Study on mechanical model of balance and stiffness characteristics of fiber reinforced bellows type rubber hose," *Sci. Adv. Mater.*, vol. 12, no. 7, pp. 981–993, Jul. 2020.
- [18] S. Huo, W. Yan, X. Xu, and Z. Yuan, "Bending characteristics of the reinforced S-shaped bellows under internal pressure," *Int. J. Pressure Vessels Piping*, vol. 192, Aug. 2021, Art. no. 104412.
- [19] S. H. Gawande and N. D. Pagar, "A combined numerical and experimental investigation on the effect of dynamics characteristics of metal expansion bellows," *J. Vibrat. Eng. Technol.*, vol. 6, no. 5, pp. 401–416, Oct. 2018.
- [20] W.-K. Shi, C. Qian, Z.-Y. Chen, Y. Cao, and H.-H. Zhang, "Modeling and dynamic properties of a four-parameter Zener model vibration isolator," *Shock Vibrat.*, vol. 2016, pp. 1–16, 2016.
- [21] D. Drotman, M. Ishida, S. Jadhav, and M. T. Tolley, "Application-driven design of soft, 3-D printed, pneumatic actuators with bellows," *IEEE/ASME Trans. Mechatronics*, vol. 24, no. 1, pp. 78–87, Feb. 2019.
- [22] M. Amritanandamayi Devi, G. Udupa, and P. Sreedharan, "A novel underactuated multi-fingered soft robotic hand for prosthetic application," *Robot. Auto. Syst.*, vol. 100, pp. 267–277, Feb. 2018.
- [23] N. Zhang, L. Ge, H. Xu, X. Zhu, and G. Gu, "3D printed, modularized rigid-flexible integrated soft finger actuators for anthropomorphic hands," *Sens. Actuators A, Phys.*, vol. 312, Sep. 2020, Art. no. 112090.
- [24] Y. Liu, M. Wang, X. Gao, and Y. Zhang, "An investigation of damping mechanism in two-layered beam with general sectional shape," *J. Vibrat. Eng. Technol.*, vol. 7, no. 2, pp. 179–188, Apr. 2019.
- [25] M. Cao, J. Zhu, H. Fu, and H. Y. F. Loic, "Response surface design of bellows parameters with negative pressure shrinkage performance," *Int. J. Interact. Des. Manuf. (IJIDeM)*, vol. 16, no. 3, pp. 1041–1052, Sep. 2022.



MIAOLONG CAO received the M.D. degree in engineering from the Zhejiang University of Technology. He is currently a Senior Technician with the School of Mechanical and Energy Engineering, Zhejiang University of Science and Technology. His research interests include mobile robotics and vehicle engineering.



YUZHOU SUN received the B.S. degree from the Xuzhou University of Technology, Xuzhou, China, in 2021. He is currently pursuing the master's degree with the College of Mechanical and Energy Engineering, Zhejiang University of Science and Technology, Hangzhou, China. His research interest includes robot control.



QINGYU DU graduated from the Department of Cultural Heritage, School of Humanities, Central Academy of Fine Arts. She is currently a Cultural Exhibition Researcher with Research and Promotion Department, Han Meilin Art Museum. Her research interests include art history and industrial design.



ZIJIAN YING completed his studies from the Zhejiang University of Science and Technology, Hangzhou, China, in 2022. He is currently pursuing the B.S. degree with the College of Computer Science, Ostfalia University of Applied Sciences, Wolfenbüttel, Germany. His research interest includes artificial intelligence.

...